Investigating a Hermetic Reciprocating Compressor Performance under Variable Lift Limiter Height using FSI Method

Aykut Bacak[a*]. Ali Pınarbaşı[a]. Ahmet Selim Dalkılıç[a]

Department of Mechanical Engineering. Faculty of Mechanical Engineering. Yildiz Technical University. 34349. Istanbul

Abstract

This groundbreaking study delves into the intricate dynamics of hermetic reciprocating compressors, highlighting the pivotal role played by mechanical, electrical, and thermal factors in shaping compressor efficiency. By employing advanced fluid-structure interaction methods, the investigation focuses specifically on discharge line energy losses, elucidating the profound impact of valve design parameters—length, thickness, and valve height—on enhancing overall compressor performance. In the development of a comprehensive 3D Fluid-Structure Interaction model, the discharge valve of a self-acting hermetic reciprocating compressor is ingeniously represented as a beam element. The utilization of the RNG k-ε model further scrutinizes the nuanced effects of reed valve thickness, length, compressor speed, and lift limiter height on pressure pulsation and, consequently, the efficiency of the compressor. Under ASHRAE conditions, operating at a challenging temperature range of 54.4°C to -23.3°C, the study meticulously explores the intricate interplay of discharge valve characteristics. Specifically, varying valve thicknesses (0.127, 0.152, 0.178, and 0.2 mm) and lengths (14.722 mm, 16.222 mm, and 17.722 mm) are examined in conjunction with different compressor speeds (1300, 2100, and 3000 rpm) according to the design specifications. Upon meticulous examination of discharge line losses at a compressor speed of 1300 rpm, intriguing insights emerged. For lift limiter heights of 0.8 mm, 1.05 mm, and 1.25 mm, coupled with a valve length of 17.722 millimeters, the study unveiled remarkable average energy losses of -6.91%, 2.83%, and -8.52%, respectively. The exploration continued at 2100 rpm, revealing a dynamic pattern with average losses for the same lift limiter heights at 0.94%, -1.26%, and -4.43%, respectively. In a succinct summary, the valve in focus demonstrated a noteworthy disparity in discharge line losses, reaching a maximum variation of 9.15%, -3.83%, and -8.30% when operated at the challenging speed of 3000 rpm.

Keywords: Hermetic reciprocating compressor, Fluid-structure interaction, Reed valve, Beam modeling, Discharge line.

Corresponding Author: A. Bacak (bacakaykut@gmail.com)

1. Introduction

Variable-speed hermetic reciprocating compressors are extensively used in various applications such as refrigeration, air compression, gas supply, and process gas compression. One common issue with these devices is the pressure pulsation that occurs due to the reed valves opening and closing periodically. This can result in compressor noise and vibration in the flow line. Furthermore, accurately predicting the thermodynamic performance of compressors is extremely challenging due to the combination of valve motion and pressure pulsation in the suction and discharge regions. To build a highly efficient refrigerator compressor, it is crucial to examine the compressor's operating course, as valve structure, lift limiter height, and rotation speed all have an impact on reciprocating compressor efficiency. The valve leaf plays a crucial role in the performance and dependability of hermetic reciprocating compressors (HRC). As a result, a considerable amount of research has been passed out to assess and increase the efficiency of valves in reciprocating compressors (RC) [1], [2].

The use of computational fluid dynamics (CFD) has progressed significantly, and it is now a valuable tool for analyzing and improving the performance of valves in hermetic reciprocating compressors. The numerical approach, specifically fluid-structure interaction (FSI), has been widely used in the past few decades to study valve motion and facilitate optimal valve design. The thermodynamic process and self-acting valve dynamics of the RC were numerically simulated by Wang et al. [3]. In the past few decades, researchers have focused on studying how different physical fields interact in compressors, with a particular emphasis on the FSI method. FSI simulations are widely used in research because they can accurately simulate fluid and valve performance as well as experimental data [4], [5]. By utilizing an FSI model to analyze the discharge valve movements in both linear and reciprocating compressors, it was determined that the leaf displacement predicted by the FSI model corresponded accurately with the observed results.

Tan et al. [6] introduced a 3-D FSI method to analyze rotary compressor discharge valve movement. A simplified cylinder form was used in a second model, which showed a partial cylinder partially covering the discharge port, causing a loss of 68.8% of flow energy. The model also indicated an angled valve reed and experimental compression chamber pressure results confirmed the FSI model's reliability in predicting valve dynamics.

Choi et al. [7] conducted a study on the steady-state properties of a valve system using ADINA software and experimental validation. They examined the dynamic characteristics of the valve system after preloading the conical compression spring. The study found that increasing the preload from 32N to 56N affected the efficiency of the linear compressor and the behavior of the valve. The timing of the discharge valve was not related to the preload, but increasing it resulted in faster closure of the discharge valve. The application of 48N preload increased the suction flow rate by 1.89% and reduced stress on the suction valve

by 4.15 percent. The ideal preload for conical compression springs is 48N for maximum suction efficiency and pressure.

Gasche et al. [8] numerically modeled the FSI problem in a suction valve shape using a three-dimensional flow and structural dynamics model. They used Ansys CFX and Ansys Mechanical's structural module for flow simulations. A 1D model was used for structure dynamics, while a 3D model was used for predicting formation deformation. The 1D model reduced computation time by 15%, while the 3D model provided more accurate design-critical data.

Gonzalez et al. [9] developed a numerical technique to evaluate the Fluid-Structure Interaction (FSI) problem in reed valves, commonly used in HRC. The technique uses a partitioned semi-implicit coupling technique, accounting for the fluid's additional mass effect, to improve numerical stability and reduce computational requirements. The reed valve is modeled using plate theory and typical mode summation, with a 3-D CFD solver for turbulent flow simulation. The study found that thinner plate thickness improves pressure drop across the valve, while valves with lower stiffness show superior suction performance.

Tao et al. [10] conducted a simulation of the complete compression cycle of an RC using a 3-D FSI model. The model accurately evaluated the thermodynamic mechanism of the compression cycle, analyzing the impact of compressor rotation speed and leaf factors on valve fluctuation and delayed closure. The FSI model identified the point at which a reed valve is defined, which maximizes delayed closure and backflow. Backflow through the valve significantly slowed compressor flow, reducing volumetric efficiency by 7% at a typical rate of 3200 r/min. The typical rotation speed was the one with the highest overdue finish and a 7% decrease in volumetric efficiency.

Kim et al. [11] use FSI analysis to simulate the motion of a discharge valve in an RC system and predict potential failure. The valve's opening and closing mechanism is influenced by the valve's motion. Before impact studies, cylinder pressure should be checked. FSI analysis provides the pre-impact state of the compressor model, estimating its dependability based on stress caused by impact phenomena. The study of a compressible model aligns with experimental testing, and FSI velocity results can predict the critical zone for potential valve failure.

Jin et al. [12] introduced the DEZ method for measuring HRC rotational speed using a three-dimensional fluid-structure interaction model. The DEZ method eliminates the tendency element of pressure pulses and isolates the current component, ensuring accurate rotational frequency determination through spectrum zooming. The method is reliable across different load scenarios, with a maximum level of inaccuracy of less than 1 rpm at 2 seconds. This method can detect the operational status of HRC, such as internal combustion engines and air compressors, even when pressure signals are unstable.

He et al. [13] used a 3D FSI method to study the performance of an HRC. They predicted low-speed compressible flow in the working fluid R600A at a cylinder pressure of 0.68 MPa and a suction pressure of 0.067 MPa. The RNG k-turbulence model was used to model flow turbulence through valves and cylinders. The study also explored the impact of polytropic exponent and refrigerant density on compressor performance. The FSI model showed that cylinder pressure and compressor performance are influenced by operating conditions, rotating speed, and refrigerant.

Yu et al. [14] developed a 3-D FSI method to analyze the dynamic performance of the valve leaf in a rotary compressor at 4800 rpm. The method evaluates the impact process, stress, and velocity on the reed's impact against the lift limiter and valve plate. The study found that the outer edge of the reed head experiences a high velocity of impact, resulting in significant stress. The findings can improve the model and crash diagnostics of the reed valve and enhance the energy effectiveness of the rotary compressor.

Kim et al. [15] used FSI analysis to predict the failure of an RC discharge valve. Cylinder pressure was confirmed before impact analysis, and the simulation reached a pressure of 1.92 MPa, similar to the experimental pressure of 1.87 MPa. The compressor had an opening speed of 7.7m/s and a closing speed of 6.4m/s, with Type 1 compressors operating at 12.4 m/s and Type 2 at 14.8 m/s. Three Type 3 compressors operated at 12 and 9.3 meters per second, opening and closing accordingly. The valve spring in Compressor Type 3 decreased the velocity at which the valve opened by pushing it forward until it reached its maximum displacement in the open position.

Wang et al. [16]'s 3D FSI model of an HRC reveals that modifying the suction valve limiter height and compressor rotational speed can affect the surface pressure circulation and dynamic properties of the reed valve. The Bernoulli effect affects the reed's surface, resulting in a low-pressure area. This low-pressure area slows valve opening but improves valve closing efficiency. It is increasing the limiter height from 2.0 to 3.6 mm delays the closing time of the suction reed valve. Lowering the limiter height increases fluid flow velocity within the narrow zone, causing the low-pressure region to become more prominent, leading to an increase in pressure differential. This results in premature shutting of the reed valve when the limiter height decreases from 2.0 mm to 1.2 mm.

Wu et al. [17] used ADINA software to verify a three-dimensional fluid-structure interaction model for investigating piston valve oscillation. They found that a suction valve mounted on the piston is more reliable due to its lower lift integral and lower effect speed on the valve plate. The piston valve lifted 4.5mm, slightly more than the standard valve's 4.44mm lift. However, the maximum valve lift was reduced. The cylinder head valve had a 4.5 percent higher ride than the piston valve. The valve opened when the charge exceeded 0.1 mm. The cylinder cover valve opened and closed at a crankshaft angle of 35.3° and 200° during suction.

Gonzalez et al. [18] conducted a 3-D CFD analysis using a large eddy simulation (LES) turbulence model. They found agreement between the model and experimental findings for variations in lift amplitude and deformation. They compared the lift, pressure, force, and effective area of a small gland valve and a larger gland valve, indicating the method accurately describes the flow field round the valve. However, a wide-ranging evaluation of the valve's interaction with other components is needed to fully understand variations in valve lift.

Rowinski et al. [19] used cartesian cut-cell finite volume to model a small displacement refrigeration compressor with small displacements. The study analyzed a HRC with a volume of 13.1 cm3 a condensing temperature of 54°C and a compressor speed of 3000 rpm. The numerical inaccuracy was low compared to pressure and valve lift measurements, and the method was more precise than the testing. The numerical approach was accurate within the examined range, despite physical models being unpredictable.

Hopfgartner et al. [20] conducted a study on a muffler neck suction valve that uses an electromagnetic coil instead of preload. The study found that completing bridge circuits with two control inputs can effectively demagnetize electromagnetic waves. The electromagnetic coil requires 2.1 watts of power at 8 volts and a duty cycle of 15%. The use of negatively pre-tensioned valves and electromagnetic coils can effectively decrease suction loss. ASHRAE achieved a power savings of 0.68 percent at a temperature range of -23°C to 55°C. The mass-flow rate in the suction port reverses, increasing from 0.26 to 1.6% and causing a decrease in the overall mass-flow rate by 0.3%. The simulation showed a 0.71 percent decrease in energy usage and a 0.32 percent decrease in cooling capacity. Admission costs were reduced by 0.39 percent in one operational circumstance and by 1.72 percent in another.

Pham et al. [21] created a 3-D CFD method for a scroll compressor, considering both the shape of the valve and multiple cross-sections. The model has minimal modelling diffusion, high precision and steadiness of orthogonal cells, and satisfactory compressor verification. The addition of revolving scrolls and reed valves is a simple task, and the experimental compressor is considered valid. The approach offers advantages such as quick conversion of CAD geometry into a CFD model, ease of modifying geometry, and simplicity of incorporating complex moving boundaries. The technique shows strong convergence, stable orthogonal cells, and satisfactory experimental data validation.

Rowinski et al. [22] validated a resistance-capacitance model using autonomous mesh creation across four operating settings. The simulation showed that refined mesh can accurately predict cylinder and discharge pressure changes. Grid discretization is more important in time-restricted scenarios. Adaptive Mesh Refinement (AMR) can improve beam, leakage, and thermal boundary conditions along the discharge flow

path. An effective approach should include adding cells in areas where the model is under-resolved or there are significant sub-grid scale fluctuations in field variables.

Bacak et al. [23] investigate energy losses in household refrigerators using an HRC. The pressure-volume indication diagram of the compressor was obtained under various operating circumstances. The study found that total compressor losses augmented with reducing condensation pressure, accounting for 10%, 8.7%, 5.7%, and 4.6% of whole work. Suction line losses, which were the largest, increased with increasing condensation pressure.

Lazoglu et al. [24] conducted a study on HRC using mathematical models and CFD simulations. They examined the impact of constant, single-variable, and double-variable coefficients on compressor performance and discharge valve displacement in three different working circumstances. The results showed that single and double-variable models accurately represented valve performance and pressure peaks, while the continuous model accurately approximated power, cooling capacity, and COP. The double variable model had the highest level of reliability in forecasting discharge losses.

This seminal investigation delves comprehensively into the intricate dynamics governing hermetic reciprocating compressors, emphasizing the pivotal influence of mechanical, electrical, and thermal parameters on the resultant efficiency of the compressor system. Employing sophisticated fluid-structure interaction methodologies, the research explicitly targets the analysis of discharge line energy losses, shedding light on the profound consequences of varying valve design parameters—specifically, length, thickness, and valve height—in augmenting the overall performance of the compressor. The study intricately develops a 3D Fluid-Structure Interaction model, ingeniously representing the discharge valve of a self-acting hermetic reciprocating compressor as a beam element. Furthermore, the application of the RNG k-ε model rigorously scrutinizes the nuanced impact of reed valve characteristics, including thickness, length, compressor speed, and lift limiter height, on pressure pulsation dynamics and, consequently, the overall efficiency of the compressor system. Operating under the challenging thermal conditions prescribed by the ASHRAE standards (54.4°C to -23.3°C), the research meticulously investigates the complex interplay of discharge valve attributes. Specifically, varying valve thicknesses (0.127, 0.152, 0.178, and 0.2 mm) and lengths (14.722 mm, 16.222 mm, and 17.722 mm) are systematically examined in conjunction with diverse compressor speeds (1300, 2100, and 3000 rpm), adhering to stringent design specifications. Energy losses are one of the parameters affecting the efficiency of a hermetic reciprocating compressor. To investigate the effect of the discharge valve on the compressor performance, valve length, thickness, and height were selected. The stiffness value of the discharge valve directly marks the operating performance of the valve and is a function of the valve mass. Since these design parameters are the parameters that affect the mass of the valve, they have an impact on the energy losses, i.e. efficiency, of the compressor.

2. Numerical model

It is commonly understood that the operation of HRCs involves a linking among the flow of refrigerant and the displacement of the valve leaf. Furthermore, the deformation of the reed valve is caused by a pressure differential, which alters the flow field of the refrigerant. Therefore, analyzing the entire operating process of an RC system is a challenging task because it requires solving the controlling equations for both the structure and refrigerant, while also taking into account their interactions. The objective of this study is to create a 3D FSI method that can be utilized to analyze compressor operation. To achieve this, the researchers utilized the industrial code CONVERGE version 2.30. The FSI study involves the separation of the HRC model into fluid and structural domains.

2.1. Fluid field and governing equations

The fluid field of the HRC model is comprised of four components: suction, cylinder, discharge, and discharge tube. Figure 1 shows that the cylinder and discharge zones are the primary locations where solid and refrigerant interact. The movement of a continuous zone of refrigerant fluid in the HRC impression was regulated by classical mechanics and thermodynamics principles. They are skilled in being described in terms of mass, momentum, and energy relationships as presented in Equations (1) - (4).

Continuity equation:

$$\frac{\partial \rho}{\partial t} + \nabla\left(\rho \vec{V}\right) = 0 \tag{1}$$

Momentum equation:

$$\rho\left(\frac{\partial \vec{V}}{\partial t} + \left(\nabla \vec{V}\vec{V}\right)\right) = -\nabla p + \nabla \tau \tag{2}$$

The stress tensor is given by:

$$\tau = \mu\left[\nabla \vec{V} + \left(\nabla \vec{V}\right)^{T}\right] - \frac{2}{3}\vec{V}I \tag{3}$$

Energy equation:

$$\frac{\partial}{\partial t}\left[\rho\left(E + \frac{1}{2}V^{2}\right)\right] + \nabla.\left[\rho V\left(E + \frac{1}{2}V^{2}\right)\right] = \nabla.\left(k\nabla T\right) + \nabla.(-pV + \tau.V) + Q \tag{4}$$

In the given equation, ρ represents density, t represents time, V represents velocity vector, τ represents the stress tensor of the fluid, E represents total internal energy, k represents thermal conductivity of the liquid, T represents thermodynamic temperature, and Q represents the specific rate of heat generation.

The Aungier-Redlich-Kwong model [26] is utilized. It is believed that R600A exhibits compressible flow with low pressure and velocity. The RNG k-ε model is utilized to model turbulent flow in the fluid domain, using the standard pressure interpolation technique. The PISO (pressure-implicit with splitting of operators) method is a solution to the issue of pressure-velocity coupling. The PISO convergence criterion multiplier, the minimum number of PISO iterations, the maximum number of PISO iterations, and PISO tolerance have been established as 20, 2, 9, and 1E-03, correspondingly.

Equations (5) to (10) represent the transport equations for turbulent energy and dissipation rate as described in reference [27].

$$\frac{\partial}{\partial t}(\rho k)+\frac{\partial}{\partial x_i}(\rho k u_i)=\frac{\partial}{\partial x_j}\left[\left(\mu+\frac{\mu_t}{\sigma_k}\right)\frac{\partial k}{\partial x_j}\right]+P_k-\rho\varepsilon \tag{5}$$

$$\frac{\partial}{\partial t}(\rho\varepsilon)+\frac{\partial}{\partial x_i}(\rho\varepsilon u_i)=\frac{\partial}{\partial x_j}\left[\left(\mu+\frac{\mu_\varepsilon}{\sigma_\varepsilon}\right)\frac{\partial \varepsilon}{\partial x_j}\right]+C_{1\varepsilon}\frac{\varepsilon}{k}P_k-C_{2\varepsilon}^{*}\rho\frac{\varepsilon^2}{k} \tag{6}$$

$$C_{2\varepsilon}^{*}=C_{2\varepsilon}+\frac{C_\mu\eta^3\left(1-\frac{\eta}{\eta_0}\right)}{1+\beta\eta^3} \tag{7}$$

$$\eta=\frac{Sk}{\varepsilon} \tag{8}$$

$$S=\sqrt{\left(2S_{ij}S_{ij}\right)} \tag{9}$$

The values of μt, which represent turbulent viscosity, are obtained by combining the related constants from the traditional k-ε model. The constants for the two models are as follows: Cμ = 0.0845, σk = 0.7194, σε = 0.7194, Cε1 = 1.42, Cε2 = 1.68, η0 = 4.38, β = 0.012.

The continuity, momentum, and energy equations can be solved using the finite-volume method. The model values are gathered at the center of each computational cell. Rhie and Chow [28] have proposed a technique that makes it possible to avoid the checkerboarding of velocity and pressure fields. This study employs variable time step values with starting, smallest, and extreme values of 1E-07, 1E-08, and 2E-06 seconds,

correspondingly. The time step has been calibrated to satisfy the CFL condition. To maintain stability and potentially increase the time step, a variable time step approach is utilized. The Courant-Friedrichs-Lewy (CFL) parameters that determine the time step are affected by various factors such as the size of the local cells, velocity, sound speed, and diffusivity. FSI events can be classified into two types: rigid-body and beam-bending. These capabilities are similar to those of both open and closed events. Translation lengths or degrees of rotation can be used to define rigid or beam FSI events as an alternative to times. During arguments, FSI events go beyond typical circumstances. The open events have disabled the use of separate triangles to make it easier to move among specific locations. Following a closure event, the presence of disconnection triangles hinders travel among different zones. Disconnected triangles activate symmetry boundary circumstances. CONVERGE does not adjust the time step to bring into line events with time steps. In conclusion, CONVERGE executes events for each time step. To accurately depict the shock in the domain caused by the closure or joining of portions, the time step is reduced by ten after an occurrence. The Successive Order Relaxation (SOR) method is utilized to solve for momentum, pressure, density, and energy. The convergence tolerances for these variables are established at 1E-05, 1E-08, 1E-04, and 1E-04, respectively.

Message Passing Interface (MPI) is used in all parallel simulations. The load balancing control utilizes Karypis' nontrivial automated domain decomposition technique [29]. When Adaptive Mesh Refinement (AMR) is used and the computational volume changes or cells are added, the spatial distribution of cells may become irregular. This study employs the Cartesian cut-cell method that was proposed by Senecal et al. [30]. The modeling process begins with a triangulated surface that accurately represents the numerical book's volume. This surface is then filled with an orthogonal basis grid size that is specified by the user. The base grid cells are partitioned into polyhedral shapes with arbitrary side lengths at the points where the triangulated face overlaps the base grid. Regardless of the size of the base grid, the volume of the cut cells will be equivalent to the significance of the original triangulated surface. Thanks to the automatic process of mesh production, minimal human intervention is required even for the most intricate boundary shapes and movements. The computational friendliness and numerical stability of this approach are enhanced by using regular orthogonal grids. The conservation equations are resolved using the finite-volume method, which is the most appropriate methodology. All the model values have been collected by accessing the center of the numerical cells.

2.2. Structure domain

The compressor model's structural field comprises the suction valve, discharge valve, valve plate, and lift limiter of the discharge valve, as illustrated in Figure 1. The FSI method utilizes a nonlinear dynamic

analysis to account for the common deformation of the reed valve. This analysis is conducted using incremental finite element equilibrium equations, which are outlined in Equation (10).

$$Mx + Cx + Kx = F_P + F_O \tag{10}$$

The matrix of constant mass is represented by M, the matrix of continuous damping is represented by C, the matrix of continual stiffness is represented by K, and the force vector at each node corresponding to the element stresses is represented by F. The symbol $\dot{x}$ is used to represent the velocity of a nodal point, while $\ddot{x}$ represents its acceleration. The incremental nodal point displacement vector is denoted by x. The model being proposed incorporates a contact condition among the reed valve and the valve seat. Stainless steel was used as the material for the reed valve in this study.

During modeling, the opening and closing values of the suction and discharge valves are defined by the user. The opening and closing values of the suction and discharge valves are defined as 1e-06 mm as far as measurable, and during the solution, if the valve opening value is greater than these values, the flow from the manifolds to the cylinder or cylinder is allowed, and vice versa, the flow from the cylinder or cylinder is not allowed. The forces on the valve, valve displacement, and velocity values are solved according to Equation (10). During the solution, suction and discharge valves are defined as Beam elements. During the valve identification, the width, thickness, type of the beam element, and the velocity, displacement, and acceleration parameters on the valve are calculated from the defined measurement point.

2.3. Modeling fluid-solid interaction

The FSI model was solved by conducting a finite volume analysis of the fluid domain using a CFD solver. On the other hand, the structural solver evaluated the solid field by utilizing a finite element-based technique. Several studies have been conducted using the FSI paradigm. The FSI solver connects the results of the two areas based on this concept. The FSI model of the compressor features three fluid-structure interfaces that connect the reed valve to the flow field. The fluid-structure boundaries comprise three components: the discharge reed valve FSI boundary, the suction reed valve FSI boundary, and the elastic damping FSI boundary. Fluid-structure boundary delineation involves the use of fluid and structural domains. The boundary of the fluid-structure interface aligns with the boundary of the structure field. To precisely obtain the pressure, temperature, and momentum changes on the refrigerant due to the movement of the solid part at the points where the moving piston and suction and discharge valves come into contact with the refrigerant, the element density in the boundary layer is increased compared to other regions by increasing the number of elements on the walls with the technique called fixed embedding. To define the

number of elements in this region, the minimum and maximum number of elements are defined on the CONVERGE software, and the number of elements on the moving parts is automatically generated by the AMR technique.

2.4. Grid independency study

The test of independence from the network structure is done to detect the network structure with the number of elements in which the results no longer change. A network structure with more elements than necessary causes the analysis time to take longer than necessary and the computer processor to be used more than necessary. In this study, the network structure independence study is based on the power consumption and mass flow rate parameters of the compressor, and the results are shown in Figure 2. In CONVERGE software, a model with a moving piston consists of static and dynamic elements. For the number of dynamic elements, a variable element range among 2000000 and 10000000 is defined, and the element is used to create the elements instantaneously during the movement of the moving piston and the opening and closing of the valves. The size of the static elements was defined as 1.5 mm and tracking was performed over this number of elements. As can be seen from Figure 2, in the case of using a network structure consisting of approximately 400000 static elements, there is no significant change in the analyzed results according to the network structure.

3. Experimental method

The thermodynamic losses of the HRC were determined by experimental measurements, ASHRAE with operational settings typical of domestic refrigerators. The coefficient of performance (COP) of a compressor is determined in basic calorimeter test unit (CTU) experiments using its cooling capacity and energy use under different working conditions. Calorimetry readings can also track the refrigerant's mass flow rate, the gas temperature at the compressor exit, and the temperatures of the enclosure face.

CTU test rigs are used to assess compressors across different operating situations. Figure 3 illustrates the cooling system and layout of the pertinent equipment used in the CTU test setup at the Arcelik R&D Center Thermodynamic Technologies Laboratory. The figure illustrates the division of the test equipment for the HRC CTU into two independent chambers. The right section contains the HRC that will undergo testing, as well as the equipment employed for tracking the suction and output pressures of those HRCs. The outstanding equipment of the cooling and measurement system is located in the left chamber, and both chambers are conditioned to keep a temperature equivalent to that of the surrounding space. Following compression in the HRC, the refrigerant vapor, which is under high pressure and high temperature, reaches the condenser. To obtain precise and reliable calorimetry data, the condensing pressure must remain

constant. Hence, a compact tubular exchanger of heat with an exceptionally high overall thermal conductivity is employed as the condenser. The condenser's thermal energy is removed by circulating cooling water via a bath with a regulated temperature.

A PID management system utilizes the condensation pressure as an input parameter to manage the electric heater in the bath. Its purpose is to keep the water temperature, and thus the condensation temperature, at the desired level. The liquid refrigerant that comes out of the condenser is gathered in a vessel known as a coil, which has a transparent glass for observation. Due to the fluctuating working conditions, the amount of refrigerant in the other system parts varies. Therefore, the battery also functions as a storage for refrigerant. The CTU test arrangement includes two subcooling devices.

The initial subcooling unit is positioned immediately before the mass flowmeter to ensure that all refrigerant accessing the flowmeter is in a condensed state. The precision of the flowmeter is diminished by the arrival of the refrigerant in the form of a liquid-steam mixture. The purpose of the second subcooling unit, located directly after the mass flowmeter, is to achieve the subcooling temperature defined by the ASHRAE standard with precision. The sizing of the heat exchanger (HE) for subcooling units and the treatment of water is similar to the conditioner mechanism for the condenser. The high-pressure refrigerant undergoes a reduction in pressure to reach the desired evaporation pressure. This is achieved by the throttling valve located in the pressure vessel (PV) within the second enclosure of the CTU test structure. Before reaching the throttling valve, the refrigerant goes throughout the condenser, coil, first subcooling unit, mass flow meter, and second subcooling unit.

The evaporation process occurs in the evaporator of the PV stated before. The PV houses an additional heat transfer (HT) medium, specifically R134a, and an electric heater located close to the liquid level of the R134a. While the system is operational, the electric heater converts the given electricity into thermal energy, which is then transmitted to the secondary fluid, resulting in the evaporation of a portion of the fluid. The secondary HT fluid undergoes condensation on the evaporator pipes located within the upper-PV. This process facilitates the exchange of thermal energy to the actual testing fluid and allows the refrigerant to undergo evaporation. According to ASHRAE standards, the superheating degree must be achieved by evaporating the secondary fluid. To accomplish this, an electrical heater is used to boost the saturation temperature of the secondary fluid to the desired superheat temperature. The high HT among the secondary fluid and the tested refrigerant helps to maintain the superheating degree. Given that the CTU volume containing the PV is kept at room temperature, it is assumed that there is no HT from the inside of the PV to its exterior. Consequently, the power provided by the electric heater is considered to be equivalent to the cooling capability of the HRC. The temperature in the areas housing the compressor, PV, and other

components is regulated to match the temperature of the entire space. The main cooling unit circulates cold water through HE and electrical heaters to carry out this process. The HEs get a continuous supply of cold water at a consistent rate. The PID control circuits, which utilize room temperatures as inputs, adjust the power of the electric heaters to sustain the desired temperature of the two volumes.

The control and recording of the operations and measurements in the CTU test apparatus are carried out utilizing a personal computer and a data capture device. The digital and analog signals of the thermocouples are captured by utilizing a commercial data capture card provided by National Instruments. The Labview® software is used to write a program that controls the entire apparatus.

The modification aims to simplify the installation of sensors that focus on the cylinder pressure and discharge valve wave of a hermetically sealed reciprocating compressor. The compressor currently has a cylinder capacity of approximately ten cubic centimeters. Table 1 displays the structural specifications of the compressor. Capturing the pV diagram during trials is challenging because of the small size of the HRC. We monitor the transient pressure record utilizing high-accuracy pressure sensors (Kulite, XT-190(M)) that have a sample rate of 50 kHz and a measuring precision of 0.1%.

The sensors are carefully equipped to match the dimensions and structure of the compressor. The sensor used to monitor suction, discharge, and cylinder pressure is incorporated into the suction plenum, cylinder, as shown in Figure 4 (a). This design ensures minimal disruption to the flow structure. This selection takes into account the seal during the transient high-pressure state and the limited installation area. The synchronized bridge module collects strain signals from the quarter bridge utilizing a strain gauge that has a measuring accuracy of 1.0%. To determine the angle of the crankshaft during the cycle, a magnetic encoder is connected to the crankshaft axis. The magnetic component of the non-contact magnetic encoder is attached to the adhesive spacer. The magnetic encoder is securely mounted on a plate in three places to prevent any influence from the rotation of the crank. Usually, the plate has three attachment points, out of which two are body holes or holes that can be drilled to the exact position, and the third one is the bolt hole located in the discharge muffler chamber. The magnetic encoder plate is securely attached to the body using studs that have the appropriate length and diameter.

4. Results and discussion

4.1. Validation of the FSI model

The experimental results of the compressor studied using the FSI method at speeds of 1300, 2100, and 3000 rpm are compared to the pV indicator diagram in Figure 5. The compression work performed by the test

and the modeling of the compression are associated under three distinct settings, as illustrated in Table 2. The maximum level of error that can happen is 2.4%. This exemplifies the reliability of the FSI structure by properly replicating the entire compression procedure.

When calculating the mass flow rate, the combination of the mass of the coolant and the graphs of the displacement of the suction and discharge valves concerning the crank angle are taken into account. The mass flow rate is calculated by taking the difference among the mass of the cylinder beforehand the suction valve is opened and the mass of the gas in the cylinder earlier the discharge valve is opened and proportioning it to one cycle time [23].

Figure 5 shows that the deviation of the cylinder pressures in the compression and expansion phases from the experimental studies increases with increasing compressor speed. It can be said that this deviation is due to the difficulty of constructing a model that is the same as the experimental study, i.e. numerical constraints, as well as the operating condition of the HRC during the experiment, as with any part of the compressor, the suction and discharge valves cannot be manufactured ideally in terms of tolerance and precision. Therefore, there may be differences among the CAD model designed in the computer environment and the valve produced according to this model, not only as a result of production but also due to defects that may occur during assembly. Therefore, these differences in-cylinder pressure in the compression and expansion phases, when considered in terms of production and assembly, suggest that there is a leakage of cylinder coolant from the suction and discharge manifolds when the valve is closed. Since the suction and discharge valves are not completely sealed, the pressure differences in the compression and expansion phases are expected and the difference among the experimental and numerical results will increase due to the increase in compressor speed.

Careful consideration of variables and their effects is necessary when comparing experimental and numerical results. The statements below demonstrate the differences among experimental and numerical findings. Measurement errors can have an impact on the results obtained through experiments due to limitations of equipment or errors made by humans during the measurement process. Mathematical models serve as the foundation for numerical simulations. However, these models often involve simplifications that may not accurately represent real-world situations. Numerical simulations may yield results that differ from experimental results. Numerical simulations involve approximations and discretization of continuous problems, which can result in errors in the numerical results. The accuracy of numerical simulations is greatly influenced by the initial and boundary conditions of the simulation. Discrepancies among experimental and numerical outcomes may arise if the simulation assumes different conditions than those present in the actual experiment. Performing simulations can be a resource-intensive and time-consuming

task. Additionally, limitations in processing power can have an adverse effect on the accuracy and precision of numerical results.

4.2. Discharge valve oscillation evaluation

The displacement of the discharge valve is measured experimentally by mounting the strain-gage sensor on the discharge valve, and in modeling studies, the displacement of the discharge valve is measured projectionally by defining a probe on a point in the center of the discharge port. During the experimental and modeling process, the displacement is obtained by taking the valve's support point as a zero reference. Figure 6 illustrates the displacement of the discharge valve for an HRC that operates at 1300 rpm. The calculation of this displacement involves the valve's thickness, length, and the height of the lift limiter. As the length of the valve increases for a thickness of 0.127 mm and all limit height values, the reed valve's fluttering movement is substituted with a more extensive opening behavior. The valve thickness value of 0.127 mm consistently demonstrates this behavior at an early stage. This indicates that reducing the thickness of the valve will also decrease the stiffness value.

As a result, the forces exerted by the refrigerant gas will surpass the inertia forces exerted by the valve. As the length of the reed valve increases from 14.722 mm to 16.222 mm, its flutter number also increases. This indicates that the 17.722 mm long valve will have a greater tendency towards complete opening. The reason for this tendency can be attributed to the amount of effort required to counteract the forces exerted by the refrigerant gas and the inertia forces of the 16.222 mm long valve.

The fluttering movement of the discharge valve is shaped by the impact of gas forces and inertia forces. It has been established that for each tested lift limiter height value, the discharge valve approaches the limit at least once. In compressors with a low lift limiter height of 0.8 mm, the valve has a limited distance to travel. As a result, the valve's fluttering movement is more noticeable, and the displacement amplitude is more significant. As the valve length increased, there was a decrease in the number of flutter movements observed. This effect was most noticeable in the compressor equipped with a high-distance lift limiter due to the greater distance of movement. Furthermore, as the length of the valve increases, the frequency of flutter movements decreases. Upon opening the discharge valve, the valve with a thickness of 0.127 mm tends to close rapidly, but it quickly reopens. This phenomenon can be described as the degree to which gas forces dominate over inertia forces in the valve. However, as the valve thickness increases, the inertia forces become more dominant than the gas forces, leading to an increase in the fluttering movement of the valve.

The discharge reed valve's opening time remains unaffected at 1300 rpm, even if there are changes made to the characteristic length, such as the valve's length and thickness, or the lift limiter height of the compressor. Upon examining the same conditions, it has been observed that the discharge valve is typically

closed at a crank angle of 360 degrees. The reed valve exhibits a notably delayed closure at a crank angle of 10 degrees. This is observed when the valve has a lift limiter height of 0.8 mm, a thickness of 0.127 mm, and a length of 17.722 mm. When the force of the refrigerant gas exceeds the inertia force of the valve, the valve remains open for a specific duration by hitting the lift limiter. The valve remains open because the gas forces are stronger than the inertia forces. These beliefs stem from the observation that the lift limiter has been struck.

Figure 7 illustrates the displacement of the discharge valve for an HRC running at 2100 rpm. At a compressor speed of 2100 rpm, the time it takes for the discharge valve to open remains constant, despite any modifications made to the valve's size, thickness, or the compressor's limiter height. Upon examination of the closing crank angle of the discharge valve, it was observed that the reed valve with a length of 17.722 mm exhibited a late closing situation. On the other hand, the valve that measures 14.722 and 16.222 mm in length and operates at a compressor speed of 1300 rpm does not encounter any delay in closing. It has been observed that the valve, which is 0.127 mm thick, has closed for the final time due to the greater force exerted by the pressure of the refrigerant gas compared to the inertia forces exerted by the valve. The discharge valve's late closing has a noticeable impact, specifically in the 17.722 mm length of the valve. When the compressor speed increases, the mass flow rate also increases. This causes an increase in gas forces, which is the most noticeable effect of the discharge valve closing later than usual. When the reed valve length of the 14.722 mm and 16.222 mm valves was increased to 17.722 mm, flutter movements were observed. However, it was also noted that the valve tended to fully open and remain open for a period of time. When the size of the reed valve is increased, it results in a larger valve displacement. This is because the reed valve covers a wider area of the valve plate, allowing a greater amount of gas to enter and exit the compression chamber. As a result, the compressor can achieve a greater displacement, leading to an increased cooling capacity.

The lift limiter height and valve displacement in HRC are interdependent. Specifically, when the lift limiter height is increased, the valve displacement decreases. To put it simply, raising the lift limiter height results in a reduction of valve displacement. The lift limiter is designed to limit the maximum height that the reed valve can reach during operation. The flow of gas into and out of the compression chamber is limited. As a result, the compressor has a reduced displacement which leads to a decrease in cooling capacity. Due to the impact of gas forces, the height of the restriction tends to decrease. The valve is more likely to stay open due to hitting the lift limiter. Furthermore, the valve may exhibit a secondary flutter motion after the initial flutter. When the limit height is lower, the movement area becomes smaller, resulting in a higher amplitude flutter movement.

When the reed valve becomes thicker, it requires more force to lift and move it. This, in turn, reduces the valve displacement and limits the amount of gas that can flow in and out of the compression chamber. As a result, the compressor has a reduced displacement, which leads to a decrease in cooling capacity. Conversely, a thinner reed valve can be lifted more easily, resulting in a greater gas flow, increased displacement, and ultimately more effective cooling capacity.

Figure 8 depicts the displacement of the discharge valve in an HRC operating at a speed of 3000 rpm. The opening time of the discharge valve remains constant for a compressor operating at 3000 rpm, irrespective of the valve's size, thickness, or limiter height. Upon investigating the timing of the closure of the discharge valve, it has been discovered that the 14.722 mm long valve closes at similar times to those of the compressor speeds of 1300 and 2100 rpm. On the other hand, the discharge valve, which measures 16.222 mm in length, experiences delays when closing. The delay in the closure of the discharge valve, which has a length of 16.222 mm, was studied and the findings indicate that a reduction in the thickness of the valve leads to an increase in the time it takings for the valve to close. The delay could potentially reach up to three degrees of crank angle. This observation is noted when the valve takes longer than anticipated to close.

Upon analysis of a valve with a length of 17.722 mm, it was found that the late shutting of the discharge valve has a relatively greater magnitude than the compressor speeds of 1300 and 2100 rpm. It was concluded that the valve closes at a crank angle of 375° when the mass flow rate increases due to the compressor's speed. This is because the gas forces are stronger than the inertia forces of the valve, and the valve has a limited range of motion with a height limit of 0.8 mm. Furthermore, the forces exerted by the gas are stronger than those exerted by the valve's inertia. At a lift limiter height of 1.05 mm, the maximum closing crank angle for a discharge valve that is 17.722 mm long is 365 degrees. Similarly, at a lift limiter height of 1.25 mm, the maximum closing crank angle is 372 degrees. It is also possible to express these angles as 360 degrees.

When observing the fluttering movement of the discharge valve, it becomes apparent that the displacement value of the second flutter movement decreases as the limit height increases. This is because the displacement value decreases as the limit height increases. The correct interpretation of the situation becomes evident upon detecting the fluttering motion of the discharge valve and increasing the lift limiter elevation results in an increase in both the flow area and the movement area of the valve. Both of these factors contribute to the phenomenon. It has been discovered that extending the length of the valve results in an increase in the second flutter displacement amplitude. In conclusion, it has been observed that the second flutter movement underwent a change in its nature and exhibited behavior similar to that of the valve's complete opening, which had the largest leaf length of 17.722 mm. This conclusion has been drawn

based on the observation of a decrease in efficiency. It has been observed that at higher compressor speeds, specifically at 3000 rpm, the valve tends to remain open. This is due to an increase in mass flow rate and gas forces as the compressor speed increases.

4.3. Discharge pressure evaluation

The pV indicator diagram of the HRC is obtained by using pressure sensors as shown in Figure 4. The pV indicator diagram shows the volume of the cylinder depending on the position of the crankshaft on the horizontal axis and the pressure in the cylinder on the vertical axis. The pressure inside the cylinder is measured during the suction, compression, discharge, and expansion phases of the compressor, and the calculation of the compressor discharge line energy losses takes into account the data of the discharge process. In summary, Figures 9-11 show the pressure measured in the cylinder during the discharge process.

The cylinder pressure in the discharge stage of an HRC analyzed at a compressor speed of 1300 rpm is presented in Figure 9. The figure has revealed that the initial opening intensity of the valve, which is also referred to as overshoot, increases as the valve length increases for a compressor valve with the same thickness, even if the lift limiter height remains constant. It has been observed that when the valve size is increased, the valve length of the cylinder pressure oscillations decreases following the overshoot. Valves with lengths of 14.722 mm, 16.722 mm, and 17.722 mm are reported to have approximately 8%, 9%, and 10% more overshoot pressure than the ideal condition for a lift limiter height of 0.8 mm. It has been discovered that the increases for the 1.25 mm limit height are 8%, 9%, and 10%, respectively. With a height limit of 1.05 mm, their heights are 8.5%, 9%, and 11.8%, respectively. Following an overshoot, there is a potential for a 10% increase in pressure fluctuation for valves measuring 14.722 mm in length, and a 12% increase for valves measuring 16.222 mm in length. Valves that are 17.722 mm in length experience a maximum pressure fluctuation reduction of 6%. Upon analyzing the influence of cylinder pressure on valve thickness at a compressor speed of 1300 rpm, it has been observed that the impact of valve thickness on overshoot is negligible across all limit height values. It has been discovered that thicker valves create a higher pressure wave due to pressure variations that occur during the discharge process following an overshoot.

The cylinder pressure in the HRC's discharge stage is depicted in Figure 10 when the compressor's speed is set at 2100 rpm. The figure has helped establish that the initial opening intensity of the valve increases as the valve length grows, even when the lift limiter height remains constant, for a compressor valve with the same thickness. To determine the answer to this question, the initial opening intensity of the valve is compared with the height of the lift limiter. Furthermore, studies have shown that increasing the valve

length of the cylinder results in a significant reduction of pressure oscillations following the overshoot. Increasing the length of the valve will lead to the following outcome. Reports suggest that valves with lengths of 14.722 mm, 16.722 mm, and 17.722 mm exhibit an overshoot pressure that is approximately 12%, 13%, and 15% higher than the optimal pressure when the maximum lift height is 0.8 mm. The estimated increases for the 1.05 mm lift limitation height are 13%, 14%, and 15%. If the lift limiter height is increased to 1.25 millimeters, the percentages for the three values become 12%, 14%, and 15%, respectively. Valves that are 14.722 mm long may experience a pressure change increase of up to 12% following an overshoot, while valves that are 16.222 mm long may experience an increase of up to 11%. Valves that have a length of 17.722 mm are capable of limiting the pressure change to a maximum of 7%.

Figure 11 illustrates the cylinder pressure in the discharge stage of the HRC compressor operating at a speed of 3000 rpm. The figure indicates that the initial opening intensity of the valve also referred to as overshoot, rises as the valve length increases for a compressor valve with the same thickness and lift limiter height. It has been observed that increasing the valve length of the cylinder can minimize pressure oscillations that occur after an overshoot, even when the valve length is increased. Valves with sizes of 14.722 mm, 16.722 mm, and 17.722 mm are reported to have approximately 18%, 20%, and 22% more overshoot pressure than the ideal condition for a lift limiter height of 0.8 mm. It has been discovered that the increases are approximately 18%, 19%, and 20% for the 1.05 mm lift limiter height. The lift limiter height of 1.25 mm varies by 18%, 20%, and 21%. Following the overshoot, the pressure variation should not exceed 4% for valves with a length of 14.722 mm and 6% for valves with a length of 16.222 mm. Following an overshoot, the pressure change is limited to a maximum increase of 4% for valves that measure 14.722 mm in length and a maximum increase of 6% for valves that measure 16.222 mm in length. Valves that have a length of 17.722 mm can experience a maximum pressure fluctuation reduction of 5%. The examination of the compressor's discharge process revealed that as the compressor speed increased from 1300 to 3000 rpm, the severity of overshoot also increased. This observation was made by evaluating the cylinder pressure. When the speed of the compressor increases from 1300 to 2100 rpm, there is a 1.7% increase in cylinder pressure. However, if the speed increases from 2100 to 3000 rpm, there is a 7% increase in cylinder pressure. As the mass flow rate increases, the overshoot effect is expected to become more pronounced. This is due to the increase in gas forces resulting from the rise in compressor speed. Upon analyzing the graphs of cylinder pressure throughout the entire discharge process, it has been observed that an increase in compressor speed leads to pressure fluctuations in the cylinder. Consequently, the valve's flutter movement frequency is reduced.

4.4. Discharge line loss evaluation

The discharge line losses of HRC can be determined by calculating the area formed by drawing a horizontal curve from the ideal condensation pressure value and the cylinder pressure curve in the discharge process on the pV diagram. Losses occur when the discharge line parts interact with the forces of the refrigerant gas. Their presence negatively impacts the functioning of the compressor and diminishes its overall effectiveness. Upon analyzing the discharge line losses for a compressor speed of 1300 rpm, it was found that the average results for limit heights of 0.8 mm, 1.05 mm, and 1.25 mm were -6.91%, 2.83%, and -8.52%, respectively. These results were obtained for a valve length of 17,722 mm. Upon calculating the figures, it has been determined that the maximum potential alterations are as follows: 7.85% increase, 12.80% decrease, and 16.43% decrease, in that order. Upon analyzing the discharge line losses of a compressor operating at 2100 rpm, it was discovered that the average losses for valve lengths of 17,722 millimeters were 0.94%, -1.26%, and -4.43% for limit heights of 0.8 mm, 1.05 mm, and 1.25 mm, respectively. The investigation findings indicate that the maximum changes observed were 9.15%, -3.83%, and -8.30%. At a compressor speed of 3000 rpm, an examination of the discharge line losses reveals that using a valve that is 17,722 mm long results in an average change of 8.60%, -2.28%, and 3.23% for limit heights of 0.8 mm, 1.05 mm, and 1.25 mm, respectively. For each limit height, a maximum change of 10.21%, -6%, and 4.76% has been identified. Upon examining all design elements, it has been demonstrated that the thickness of the valve is directly proportional to the increase in the amount of discharge line losses. It has been determined that when the thickness of the valve increases, the forces exerted by the refrigerant gas become weaker than the forces exerted by the valve's inertia.

5. Conclusion

The study focused on analyzing the discharge process of a hermetic reciprocating refrigerator compressor by examining discharge line losses, discharge valve displacement, and cylinder pressure. The research utilized the FSI technique and evaluated compressor speeds of 1300, 2100, and 3000 rpm under ASHRAE operating conditions of 54.4°C/-23.3°C. By utilizing the third approach described in the literature, it is possible to construct the mesh structure of these complex designs without any supplementary time or effort. Therefore, this approach requires significantly less time compared to other methods for developing the model and finding the solution. The CONVERGE software performs the required calculations for the compression process, which includes the reed valve of the reciprocating compressor. The purpose of this paper is to introduce an FSI approach that can be used to analyze the thermodynamic process and valve motion of an HRC. This work was carried out by the authors. The FSI method is used to examine the four steps of the compressor: suction, compression, discharge, and expansion. This involves considering the interaction among the refrigerant and the moving solid elements. This research is unique in that it extensively examines the movements of the discharge valve and the cylinder pressure during the discharge

process, setting it apart from previous studies. Based on the findings of the numerical model, it can be concluded that the pressure fluctuations within the cylinder are reliable. The summary of the conclusions is provided below:

a) It has been discovered that the FSI tool is proficient of realistically modelling the suction, compression, discharge, and expansion of the HRC. This is achieved by taking into account the interaction among the refrigerant and solid components such as the valve and piston. The results obtained from this simulation are in close agreement with experimental results.
b) It has been established that an increase in valve thickness results in higher discharge line losses for the compressor. When the thickness of the valve increases, the inertia forces of the valve also increase. As a result, these forces become more significant than the gas forces, the reverse flows in the port and plenum due to the valve's interaction with the refrigerant, and the losses caused by effects such as post-port returns.
c) It is not possible to directly determine how the restriction height affects the losses in the discharge line. It has been determined that the compressor's discharge line losses can be reduced by designing the discharge line with an appropriate restriction height, valve thickness, valve length, and compressor speed.
d) While it was not possible to establish a direct correlation between the valve length and the discharge line losses, it was found that increasing the valve length from 14,722 mm to 16,222 mm increased discharge line losses. However, when the valve length was further increased from 16,222 mm to 17,722 mm, the discharge line losses decreased.
e) It has been determined that the discharge line losses increase as the compressor speed increases, provided that all other parameters remain constant. It has been determined that losses increase as the velocity of the refrigerant and gas forces increase, while the design parameters remain stable.
f) As the speed of the compressor increases, the flutter number of the discharge valve decreases. The decrease mentioned here indicates that the leaf tends to remain fully open instead of oscillating. It has been observed that this tendency becomes more prominent with an increase in the speed of the compressor.
g) It has been determined that increasing the compressor speed results in an increase in the intensity of the overshoot and the first opening characteristic of the discharge valve. The intensity of overshoot in compressors used in household refrigerators is a condition that raises the discharge line losses of the compressor, leading to a reduction in its efficiency. Although the desired effect may be achieved, it is important to note that its impact is likely to be minimal. Research has shown that the extent of this effect increases in direct correlation with the valve's length.

6. Acknowledgement

The authors express their gratitude to Arcelik A.Ş. for their assistance during the experimental investigation. This research is grounded on the doctoral dissertation from Yildiz Technical University. For this project, CONVERGE was supported by Convergent Science through licensing and technical assistance.

Nomenclature

C_m	Mass damping coefficient
E	Total internal energy
ε	Turbulence dissipation rate
F_P	Force due to pressure
F_O	Other forces
I	Turbulence intensity
k	Turbulence kinetic energy
K	Stiffness damping coefficient
k	Thermal conductivity
M	Mass
Q	Specific rate of heat generation
P	Pressure
ρ	Density
t	Time
T	Thermodynamic temperature
τ	Stress tensor
μ	Dynamic viscosity
V	Velocity

x	Distance
$\dot{x}$	Speed
ẍ	Acceleration

Abbreviations

AMR	Adaptive mesh refinement
ASHRAE	American society of heating, refrigerating, and air-conditioning engineers
BDC	Bottom dead center
CFD	Computational fluid dynamics
CTU	Calorimeter test unit
DEZ	Detrending extracting zooming
FSI	Fluid-structure interaction
HT	Heat transfer
HE	Heat exchanger
LES	Large eddy simulation
PISO	Pressure-implicit with the splitting of operators
pV	Pressure-volume
PV	Pressure vessel
RNG	Renormalization group
rpm	Rotation per minute

REFERENCES

[1] Wang. F., Mu. G., & Guo. Q. (2016). Design optimization of compressor reed valve based on axiomatic design. International journal of refrigeration. 72. 132-139.

[2] Ma. Y. He. Z. Peng. X. & Xing. Z. (2012). Experimental investigation of the discharge valve dynamics in a reciprocating compressor for the trans-critical CO2 refrigeration cycle. Applied Thermal Engineering. 32. 13-21.

[3] Wang. Y. Feng. J., Zhang. B. & Peng. X. (2013). Modeling the valve dynamics in a reciprocating compressor based on two-dimensional computational fluid dynamics numerical simulation. Proceedings of the Institution of Mechanical Engineers. Part E: Journal of Process Mechanical Engineering. 227(4). 295-308.

[4] Mayer. J., Bjerre. P., & Brune. F. (2014). A comparative study of different numerical models for flapper valve motion.

[5] Hwang. I. S. Park. S. J., Oh. W., & Lee. Y. L. (2017). Linear compressor discharge valve behavior using a rigid body and FSI valve models. International Journal of refrigeration. 82. 509-519.

[6] Tan. Q. Pan. S. L., Feng. Q. K., Yu. X. L., & Wang. Z. L. (2015). Fluid–structure interaction model of dynamic behavior of the discharge valve in a rotary compressor. Proceedings of the Institution of Mechanical Engineers. Part E: Journal of Process Mechanical Engineering. 229(4). 280-289.

[7] Choi. Y. S., Lee. J. H., Jeong. W. B., & Kim. I. G. (2010). Dynamic behavior of valve system in linear compressor based on fluid-structure interaction. Journal of mechanical science and technology. 24(7). 1371-1377.

[8] Gasche. J. L., Dias. A. D. S. D. L., Bueno. D. D., & Lacerda. J. F. (2016). Numerical simulation of a suction valve: comparison between a 3D complete model and a 1D model.

[9] Gonzalez. I., Lehmkuhl. O., Naseri. A., Rigola. J., & Oliva. A. (2016). Fluid-structure interaction of a reed-type valve.

[10] Tao. W., Guo. Y., He. Z., & Peng. X. (2018). Investigation on the delayed closure of the suction valve in the refrigerator compressor by FSI modeling. International Journal of Refrigeration. 91. 111-121.

[11] Kim. H., Ahn. J., & Kim. D. (2008). Fluid-structure interaction and impact analyses of reciprocating compressor discharge valve.

[12] Jin. H., Sun. Z., Gu. J., Huang. Y., Wang. X., Zhang. Q., & Shen. X. (2020). A detrending-extracting-zooming-based speed measurement method for hermetic reciprocating compressor. Measurement. 157. 107654.

[13]He. Z., Jian. Z., Wang. T., Li. D., & Peng. X. (2017. August). Investigation of the variation of pressure in the cylinder of the refrigerator compressor based on FSI model. In IOP Conference Series: Materials Science and Engineering (Vol. 232. No. 1. p. 012005). IOP Publishing.

[14]Yu. X., Tan. Q., Ren. Y., Jia. X., & Jin. L. (2017). Numerical study of the reed valve impact in the rotary compressor by FSI model. Energy Procedia. 105. 4890-4897.

[15] Octavianty. R., Kim. D. H., Park. K. G., Jung. W. H., Ahn. J. W., Moon. K. H., ,. & Kim. H. S. (2007). Flow structure interaction 3-D reciprocating compressor and impact analyses of compressor discharge valve. In Proceedings of the Korean Society for Noise and Vibration Engineering Conference (pp. 633-640). The Korean Society for Noise and Vibration Engineering.

[16]Wang. Y., Wang. J., He. Z., Sun. J., Wang. T., & Liu. C. (2021). Investigation on Dynamic Characteristics of the Reed Valve in Compressors Based on Fluid-Structure Interaction Method. Applied Sciences. 11(9). 3946.

[17] Wu. W., Guo. T., Peng. C., Li. X., Li. X., Zhang. Z., ,. & He. Z. (2022). FSI simulation of the suction valve on the piston for reciprocating compressors. International Journal of Refrigeration. 137. 14-21.

[18] González. I., Naseri. A., Rigola. J., Pérez-Segarra. C. D., & Oliva. A. (2017. August). A fluid-structure interaction solver for the fluid flow through reed type valves. In IOP Conference Series: Materials Science and Engineering (Vol. 232. No. 1. p. 012032). IOP Publishing.

[19] Rowinski. D. H., & Davis. K. E. (2016). Modeling reciprocating compressors using a Cartesian cut-cell method with automatic mesh generation.

[20] Hopfgartner. J., Posch. S., Zuber. B., Almbauer. R., Krischan. K., & Stangl. S. (2017. August). Reduction of the suction losses through reed valves in hermetic reciprocating compressors using a magnet coil. In IOP conference series: materials science and engineering (Vol. 232. No. 1. p. 012034). IOP Publishing.

[21] Pham. H. D., Brandt. T., & Rowinski. D. H. (2018). Modeling A Scroll Compressor Using A Cartesian Cut-Cell Based CFD Methodology With Automatic Adaptive Meshing.

[22] Rowinski. D. H., Sadique. J., Oliveira. S. J. D., & Real. M. (2018). Modeling A Reciprocating Compressor Using A Two-Way Coupled Fluid And Solid Solver With Automatic Grid Generation And Adaptive Mesh Refinement.

[23] Bacak, A., Pınarbaşı, A., & Dalkılıç, A. S. (2023). An experimental study on the determination of a hermetic reciprocating compressor's discharge and suction losses. Proceedings of the Institution of Mechanical Engineers, Part E: Journal of Process Mechanical Engineering, https://doi.org/10.1177/09544089231154350

[24] Pashak, P., Karabay, A. Y., Sahin, C., Malik, A. N., & Lazoglu, I. (2023). Comparison of constant and variable discharge flow and force coefficients for reciprocating compressor. International Journal of Refrigeration.

[25] Bacak, A., Pınarbaşı, A., & Dalkılıç, A. S. (2023). A 3-D FSI simulation for the performance prediction and valve dynamic analysis of a hermetic reciprocating compressor: une simulation fsi 3d pour la prédiction des performances et l'analyse dynamique des vannes d'un compresseur hermétique. International Journal of Refrigeration. https://doi.org/10.1016/j.ijrefrig.2023.01.028

[26]Redlich. O., & Kwong. J. N. (1949). On the thermodynamics of solutions. V. An equation of state. Fugacities of gaseous solutions. Chemical reviews. 44(1). 233-244.

[27] Yakhot. V., & Orszag. S. A. (1986). Renormalization group analysis of turbulence. I. Basic theory. Journal of scientific computing. 1(1). 3-51.

[28]Rhie. C. M., & Chow. W. L. (1983). Numerical study of the turbulent flow past an airfoil with trailing edge separation. AIAA journal. 21(11). 1525-1532.

[29]Karypis. G., 1998. A software package for partitioning unstructured graphs. partitioning meshes. and computing fill-reducing orderings of sparse matrices.

[30]Senecal. P. K., Richards. K. J., Pomraning. E., Yang. T., Dai. M. Z., McDavid. R. M., .,. & Shethaji. T. (2007). A new parallel cut-cell Cartesian CFD code for rapid grid generation applied to in-cylinder diesel engine simulations (No. 2007-01-0159). SAE Technical Paper.

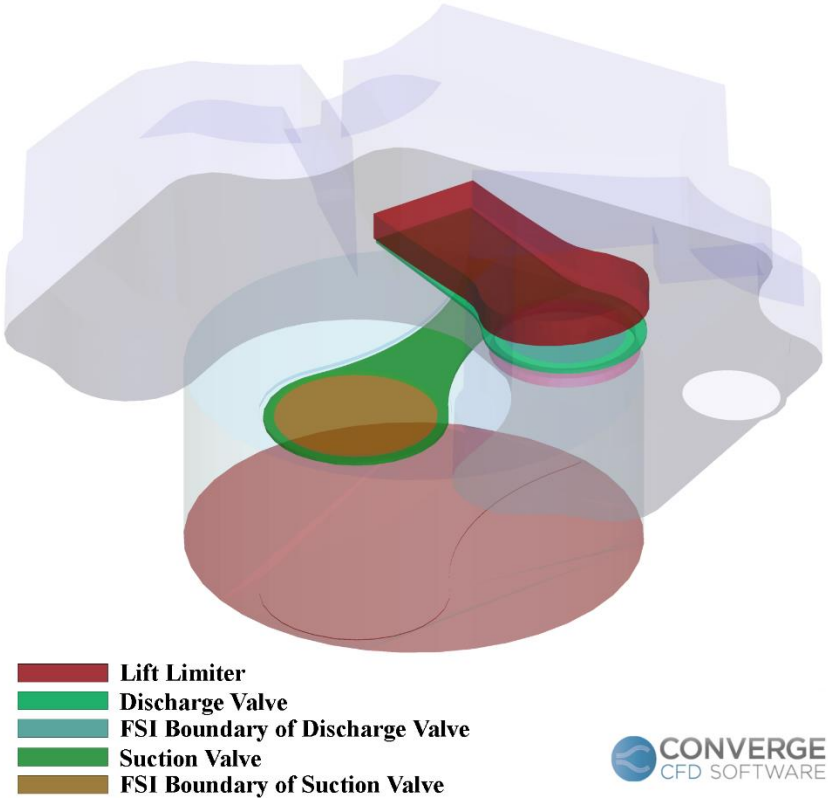


Figure 1. Model of compressor fluid domain.

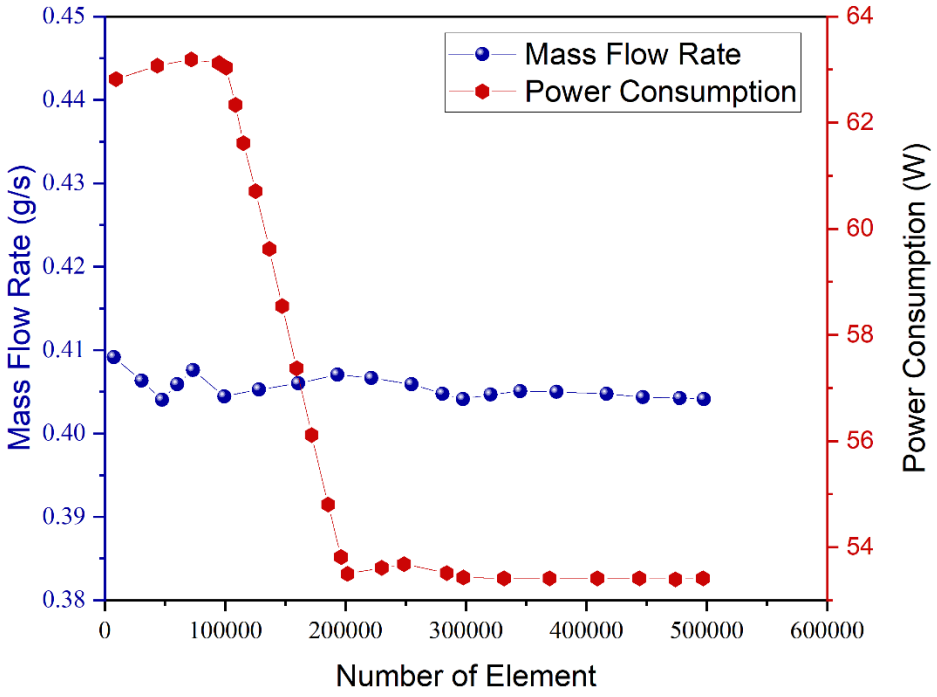


Figure 2. Grid independency study

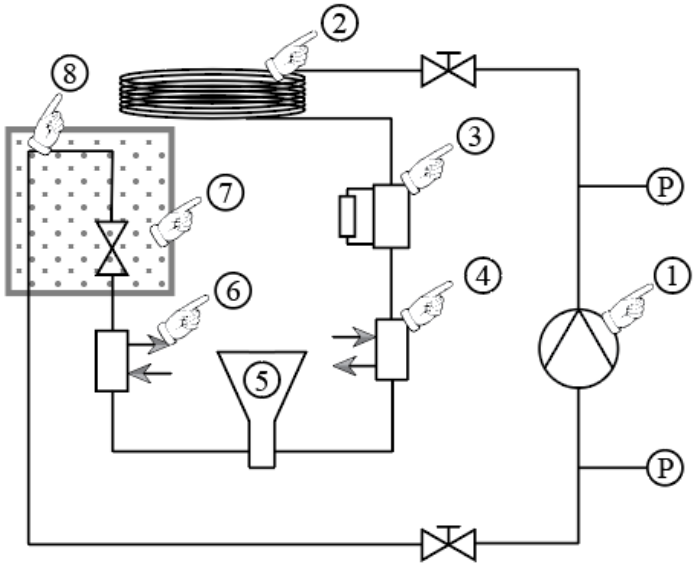


Figure 3. Schematic view of the used calorimeter test unit: (1) compressor, (2) condenser, (3), accumulator, (4) 1st subcooler unit, (5) flowmeter, (6) 2nd subcool unit, (7) expansion valve, (8) evaporator From Bacak et al. [23] with permission from Sage Publishing.

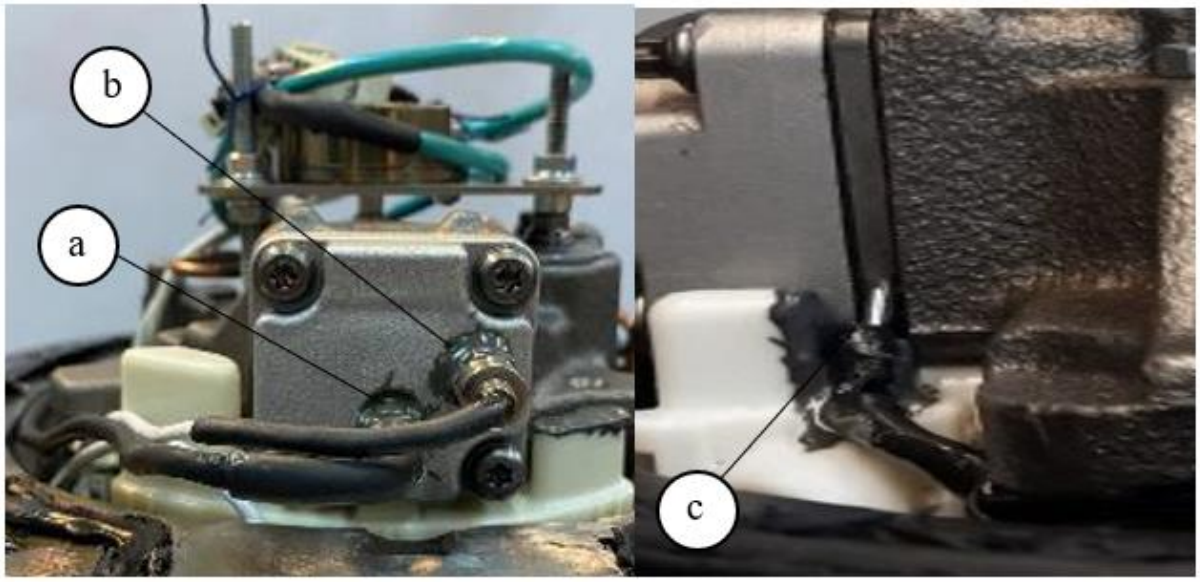


Figure 4. The installation of the suction, discharge, and cylinder pressure sensors (a) suction pressure, (b) discharge pressure, (c) cylinder pressure From Bacak et al. [25] with permission from Elsevier.

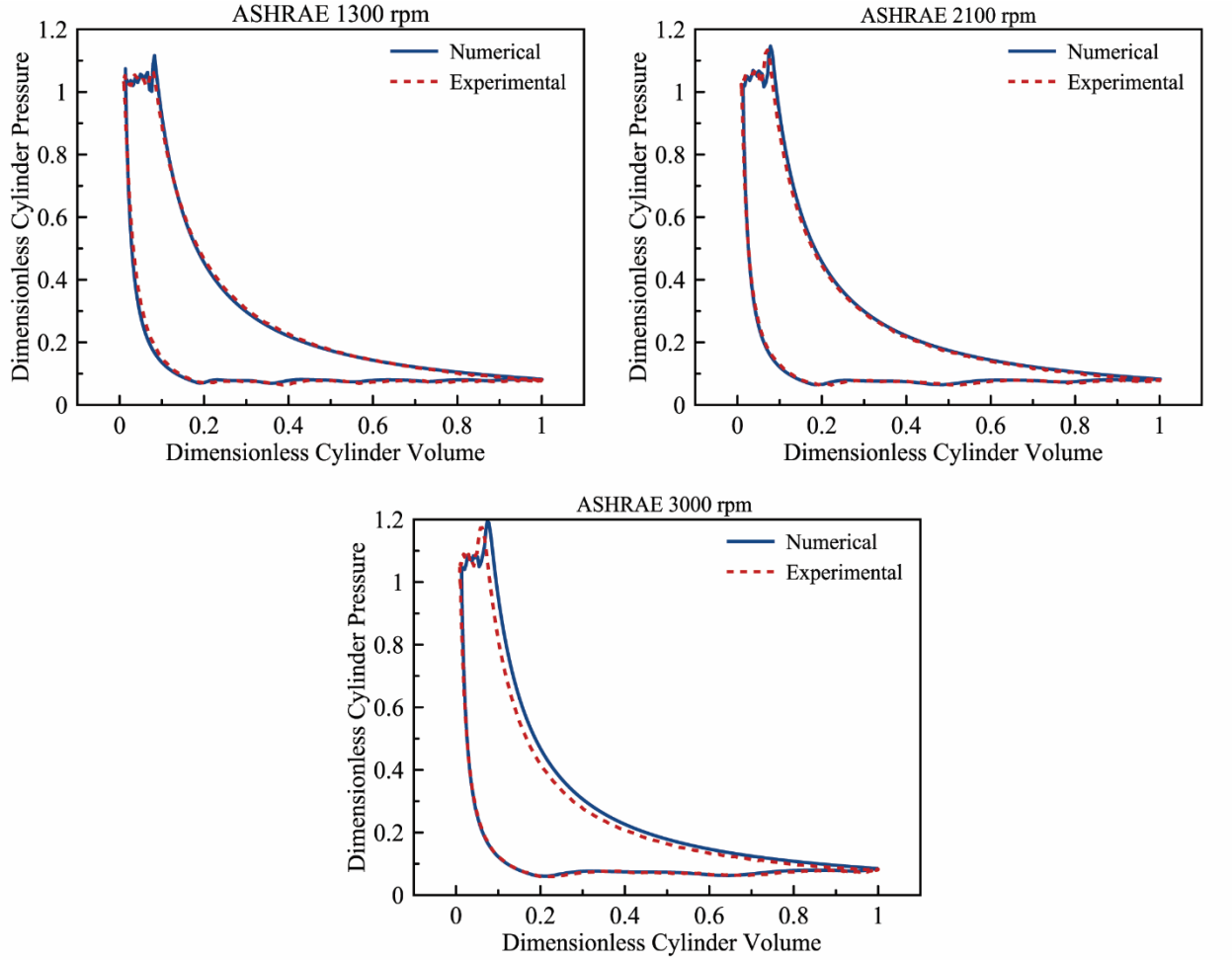


Figure 5. Comparisons of numerical and experimental outputs for 1300. 2100. and 3000 rpm. respectively

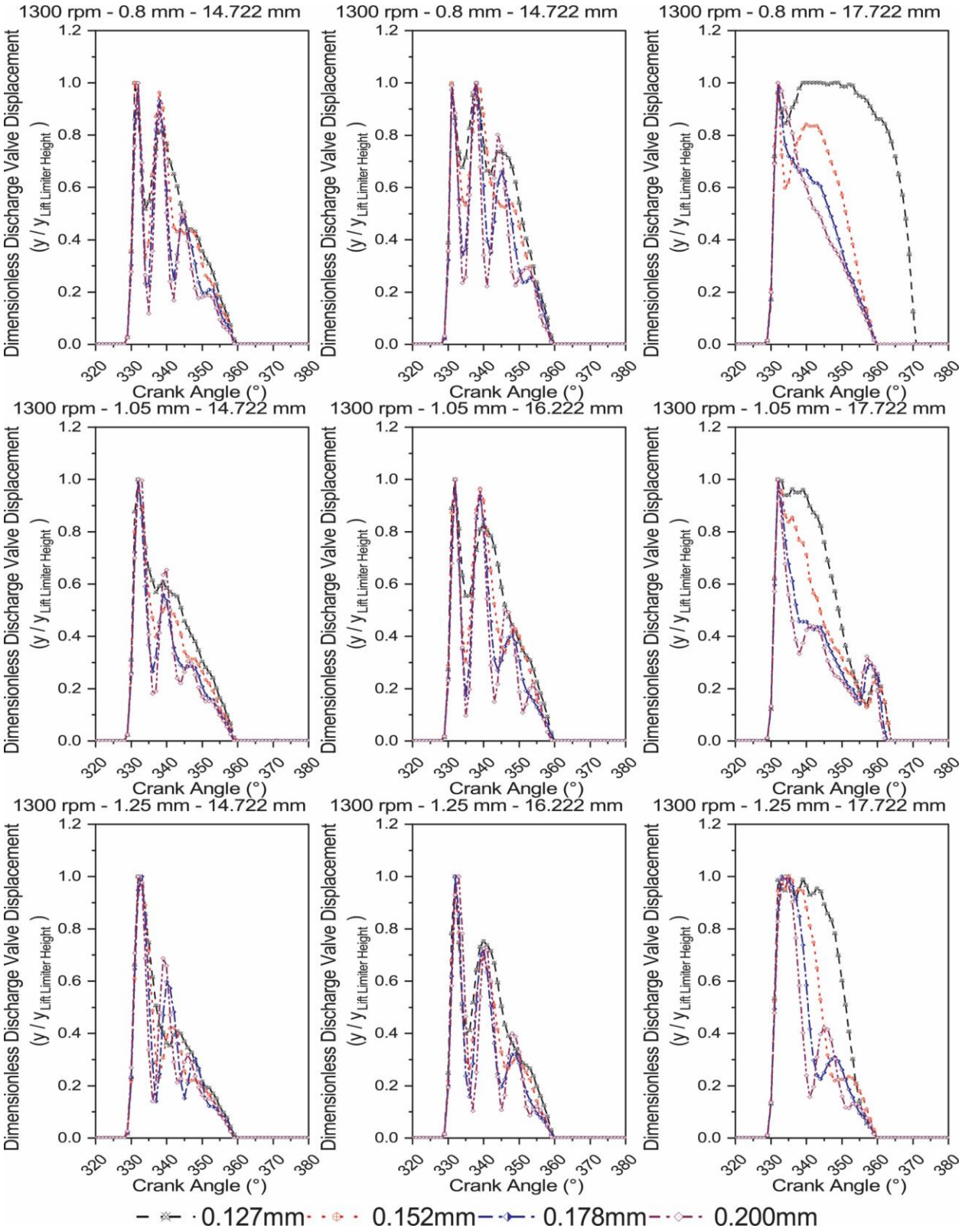


Figure 6. Discharge valve displacement results for 1300 rpm compressor speed

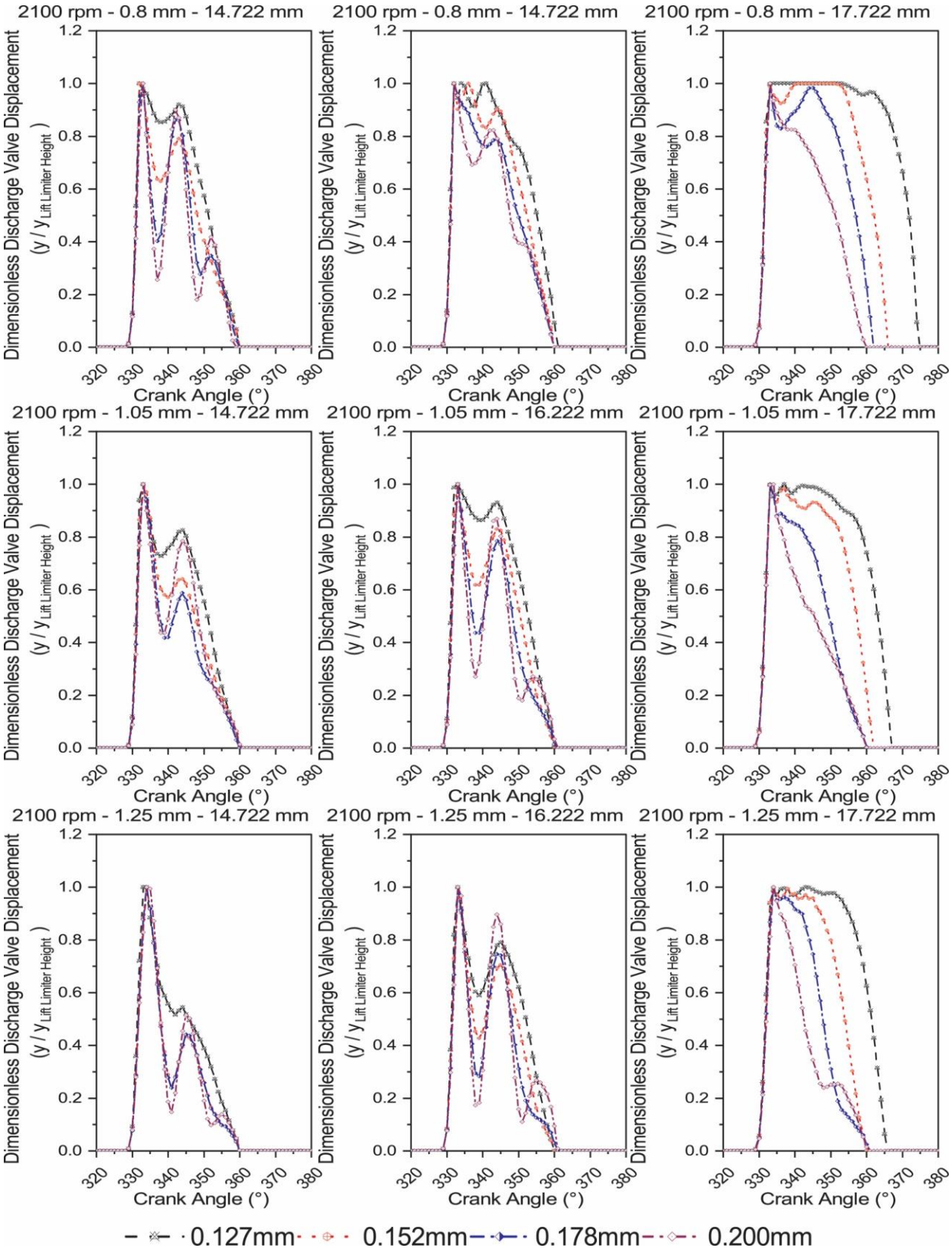


Figure 7. Discharge valve displacement results for 2100 rpm compressor speed

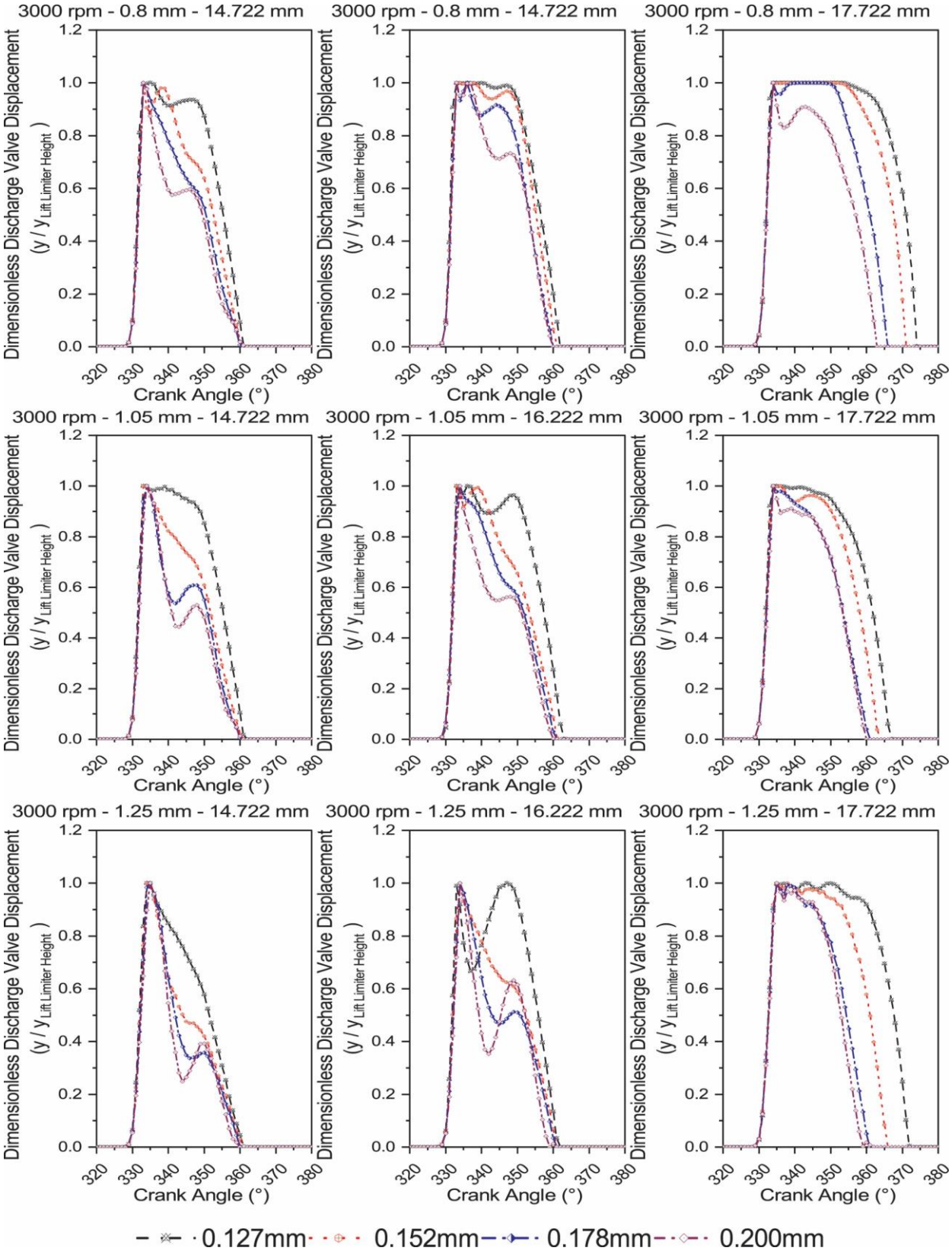


Figure 8. Discharge valve displacement results for 3000 rpm compressor speed

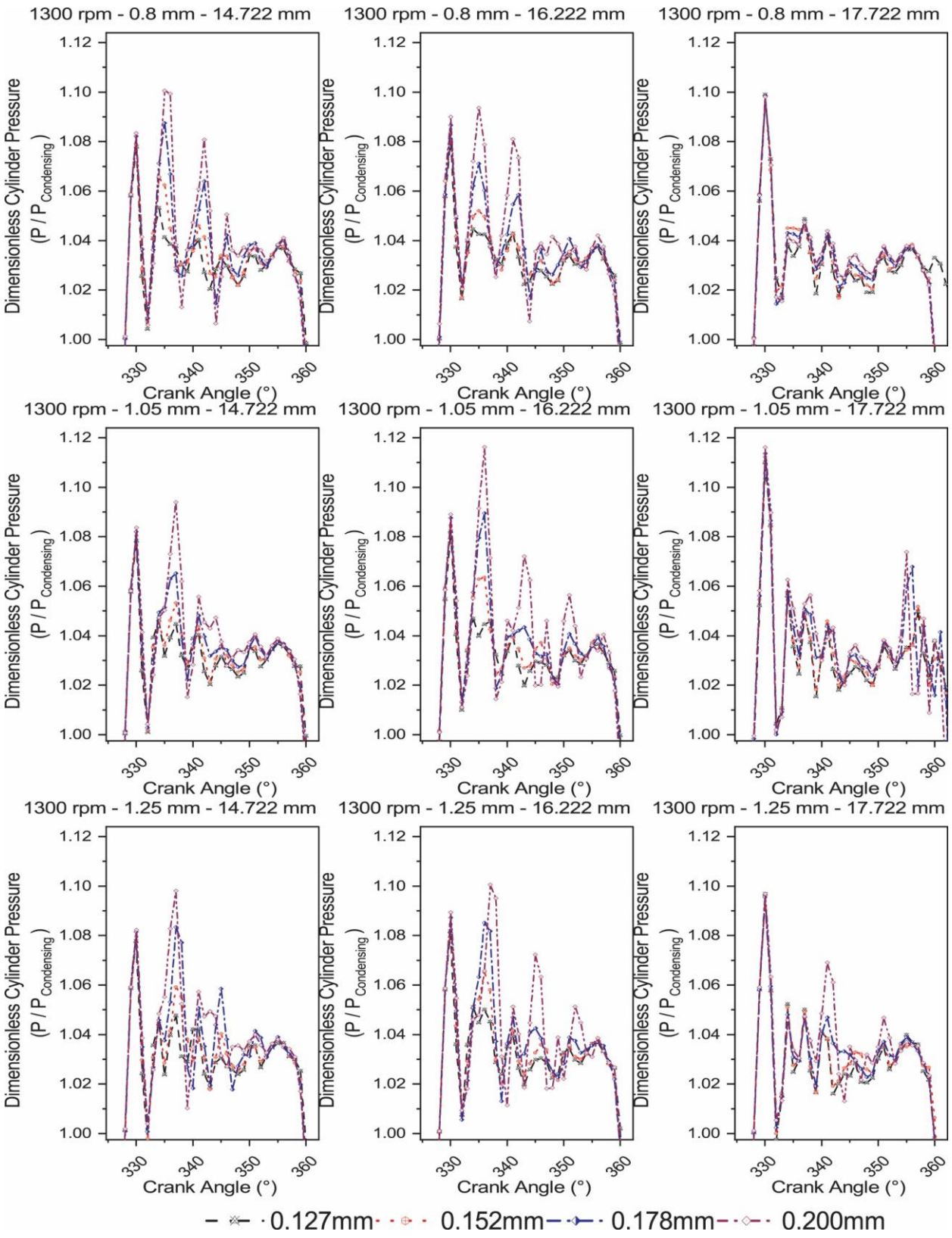


Figure 9. Discharge section of cylinder pressure for 1300 rpm compressor speed

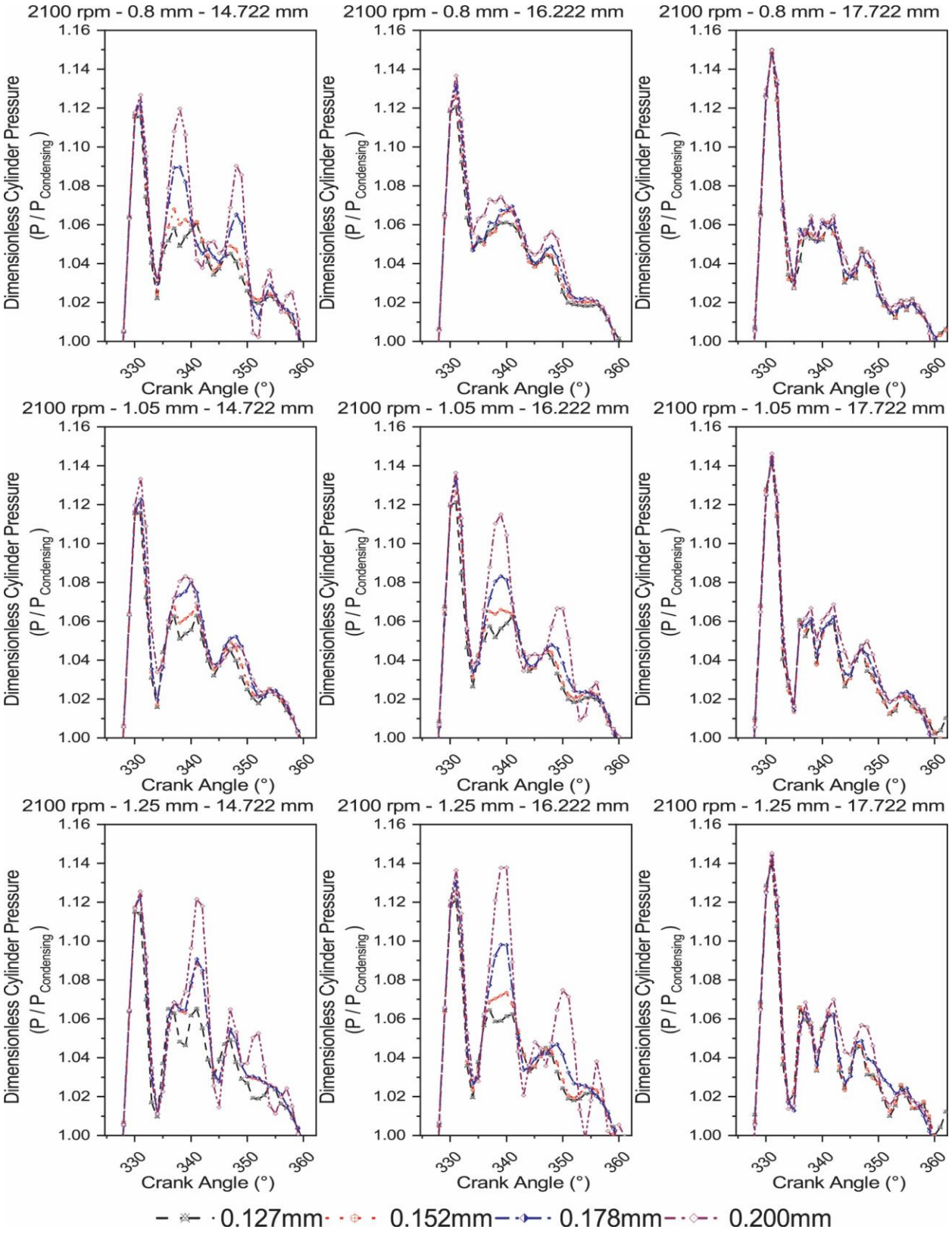


Figure 10. Discharge section of cylinder pressure for 2100 rpm compressor speed

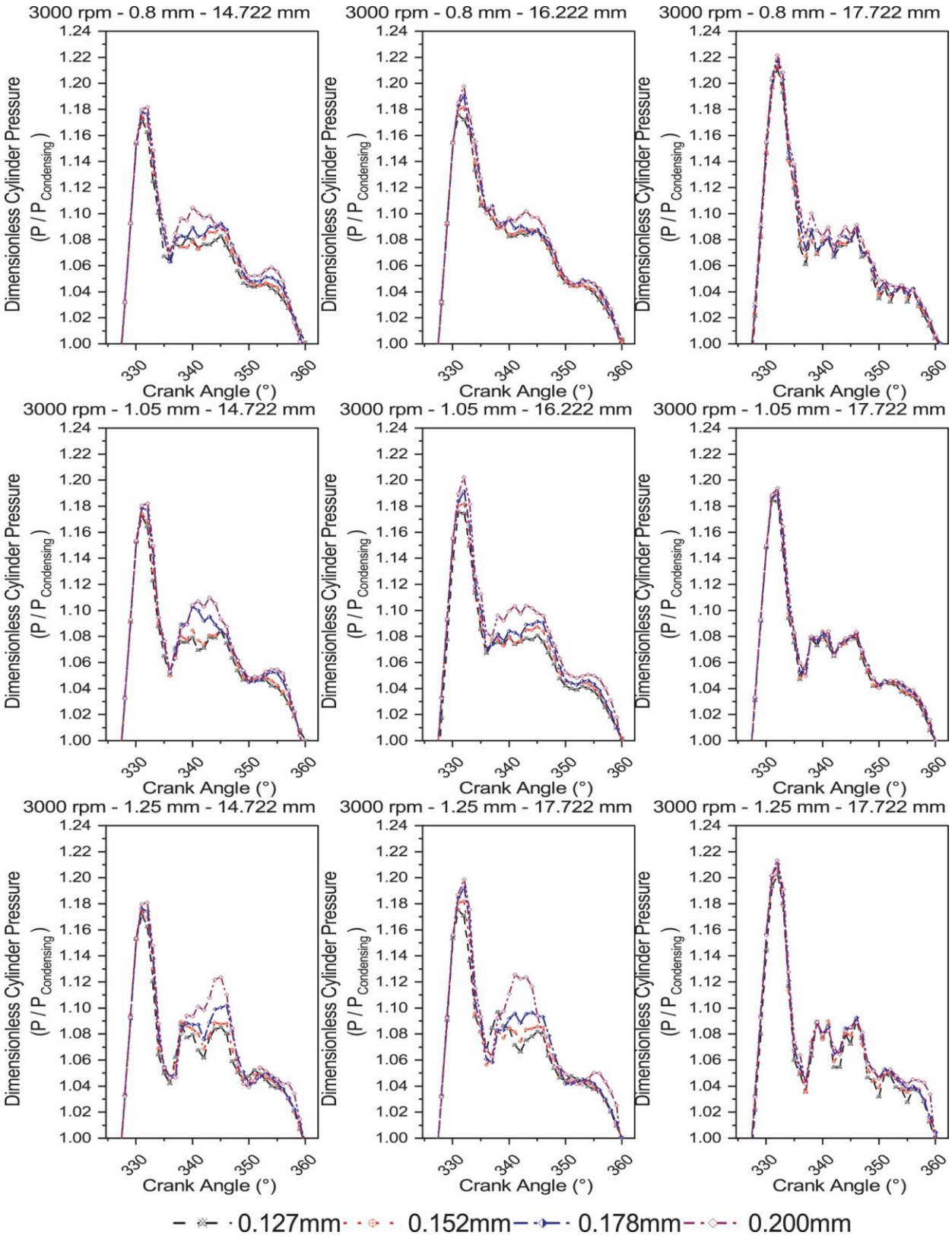


Figure 11. Discharge section of cylinder pressure for 1300 rpm compressor speed

Table 1. Design parameters of an investigated compressor

Design Parameter	Value
Cylinder bore	24.28 mm
Crankshaft diameter	10.64 mm
Eccentricity	2.75 mm
Connection rod length	38.7 mm
Oil viscosity	10 cSt
Reed valve thickness	0.2 mm

Table 2. Validation results of compressor work and inner mass flow rate From Bacak et al. [25] with permission from Elsevier.

Operating condition	Speed	Numerical		Experimental		Differences in compressor work	Difference of mass flow rate
		Compressor work	Mass flow rate	Compressor work	Mass flow rate		
	rpm	W	g/s	%	g/s	%	%
ASHRAE (54.4°C/-23.3°C)	2100	52.99	0.360	52.09	0.355	1.79	-1.28
(25°C/-20°C)	1300	26.43	0.321	26.59	0.319	-0.6	0.6
(40°C/-25°C)	1600	33.79	0.282	34.97	0.289	3.4	2.4